Proceedings of the IASS 2024 Symposium
Redefining the Art of Structural Design
August 26-30, 2024, Zurich Switzerland
Philippe Block, Giulia Boller, Catherine DeWolf,
Jacqueline Pauli, Walter Kaufmann (eds.)

A novel shape optimization framework for cast steel tubular joints

Xiaonong GUO*, Gen LI

* College of Civil Engineering, Tongji University
NO.1239 Siping Road, Shanghai, China
guo-xiao-nong@tongji.edu.cn

Abstract

Cast steel tubular (CST) joints are extensively employed in spatial trusses, grid shells, and tree-like structures, owing to their advantages of excellent mechanical properties. However, the diverse configurations of CST joints result in the lack of verification formulas within the design codes, leaving engineers reliant on trial-and-error design approaches. To address this issue, a novel shape optimization framework is proposed, combining the subdivision surface and the genetic algorithm to streamline the CST joint design process. The proposed framework encompasses three modules: geometric modeling, structural analysis, and optimization algorithm modules, with shape optimization tasks completed through their synergetic operations. The proposed framework is verified against two numerical examples and achieves a 62.3% reduction in the maximum Mises stress and a 56.5% decrease in the strain energy in the two examples respectively. The proposed method can improve the mechanical performances of CST joints and provide joint design schemes with continuous and smooth surfaces. Furthermore, this method is also highly automated and can enhance design efficiency by reducing manual efforts in the design process.

Keywords: Cast steel tubular joints, shape optimization, subdivision surface, genetic algorithm

1. Introduction

The cast steel tubular (CST) joint is a prevalent joint form in steel structures, widely utilized in projects such as tree-like and grid shell structures [1], [2]. CST joints offer superior integrity compared to welded joints, circumventing issues such as material shrinkage and stress concentration arising from welding [3], [4]. However, the diverse configurations of CST joints lead to the lack of universal verification formulas, forcing designers to depend on finite element analysis for safety assessments. Generally, design schemes must undergo iterative modifications until they meet safety standards, which is rather time-consuming and labor-intensive.

Topology optimization (TO) techniques have been applied to the design of CST joints [5]-[9]. While TO methods can effectively reduce structural weight and enhance performance, they come with several limitations. First, structures optimized via TO methods often exhibit irregular geometries, necessitating fabrication through 3D printing technology [10]. However, large-scale metal 3D printing is not mature yet [5], limiting its practical engineering application. Second, TO can result in rough surfaces and minuscule structural features, making tedious post-processing necessary to achieve reasonable designs [11], thereby increasing both time and labor costs. Finally, while structural stress is a critical concern for designers, current TO approaches usually focus on minimizing strain energy, leaving stress-oriented optimization with challenges [12].

Shape optimization is a structural optimization technique that modifies only the geometric boundaries of structures [13], thereby maintaining the structure's original topology and circumventing the manufacturability issues associated with topology optimization. The first and most important step of shape optimization is to determine the geometric representation approach of structures. In the early stages of shape optimization, the finite element mesh was utilized to represent the shape of structures,

while the shape was adjusted by moving the boundary nodes of the finite element mesh [14]. While straightforward, this approach could lead to jagged geometric boundaries and mesh distortion which might abort the optimization process [15]. With the advancement of geometric modeling technologies, various methods such as polynomials, B-splines, and non-uniform rational B-splines (NURBS) have been incorporated into shape optimization research [16]-[18]. Among these, NURBS surfaces have become the most popular method, due to their merits of flexibility, continuity, and smoothness. However, the tensor product structure of NURBS surfaces poses significant difficulties in representing topologically complex surfaces, making them unsuitable for the shape optimization of CST joints. In summary, existing methods each have notable limitations when applied to CST joints, indicating an urgent need for novel approaches.

In response, this study introduces the subdivision surface technique to the shape optimization of CST joints. This method, initially proposed by Chaikin et al. [19] and subsequently developed by Loop [20], Doo and Sabin [21], Catmull and Clark [22], and others, begins with a basic control mesh that is iteratively subdivided to achieve an approximately smooth surface. The ability of subdivision surfaces to represent geometries with arbitrary topologies makes them particularly suited for the complex shapes of CST joints.

In this study, the geometric modeling of CST joints is established based on the subdivision technique, while the positions of control mesh vertices serve as design variables of the optimization problem. Subsequently, structural analysis for CST joints is automated through secondary development in Abaqus software. Finally, the genetic algorithm is employed to adjust the position of the control mesh vertices and optimize the shape of CST joints. The remainder of this paper is organized as follows: Chapter 2 details the proposed shape optimization framework for CST joints; Chapter 3 illustrates the practical application of this framework using two numerical examples; and Chapter 4 concludes the study while suggesting directions for future research.

2. Shape optimization framework for CST joints

2.1. General introduction

The proposed shape optimization framework for CST joints, depicted in Figure 1, comprises three main modules: optimization algorithm, geometric modeling, and structural analysis. The optimization algorithm module is responsible for performing the genetic algorithm, which initiates the optimization process by generating the initial population and specifying the geometric parameters. The geometric modeling module then processes these parameters to construct and export the geometric models of CST joints. Following this, the structural analysis module imports these models to perform finite element analysis and extracts the results. The optimization algorithm then evaluates these results to assess the fitness of each solution and applies genetic operations to produce the subsequent generation. This cycle continues until the stop criterion is reached. Details regarding the geometric modeling, structural analysis, and optimization algorithm modules are provided in Sections 2.2, 2.3, and 2.4, respectively.

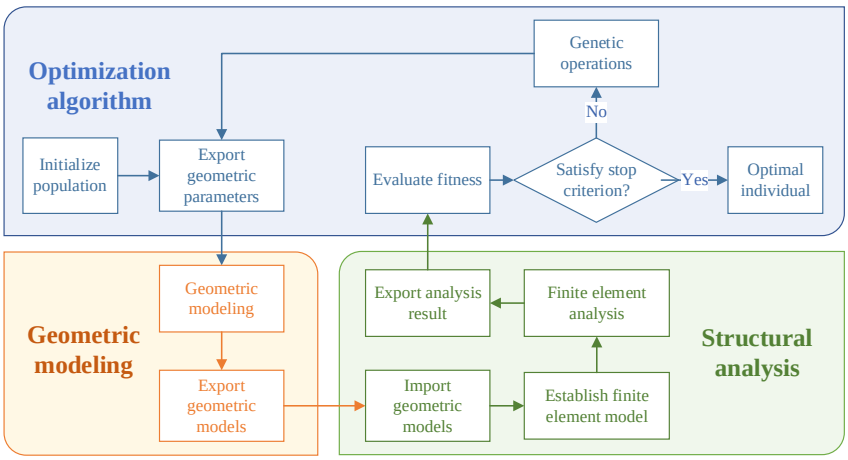

Figure 1 Flow chart of the shape optimization framework

2.2. Geometric modeling

Based on the Rhino Grasshopper platform, the geometric modeling module for CST joints is established, and its process is illustrated from Figure 2 to Figure 4. Within Grasshopper, the MultiPipe component can create a smooth surface for intersecting pipes based on the subdivision surface technique. Initially, this component is employed to generate the initial joint shape, from which the control mesh is then extracted, as shown in Figure 2. Subsequently, the vertices of the control mesh are moved to modify the joint's shape. To ensure maximum shape modification, the vertex movement is constrained to its normal direction. Additionally, to preserve joint connectivity with adjacent members, vertices on the mesh boundary are fixed, allowing only the internal vertices to be adjusted, as displayed in Figure 3. Once all vertices are moved to the designated positions, the deformed control mesh is subdivided and the geometric model for the CST joint is obtained, as illustrated in Figure 4.

(a) Axes and diameters (b) Subdivision surface (c) Control mesh

Figure 2 Initial joint shape construction with Multipipe component

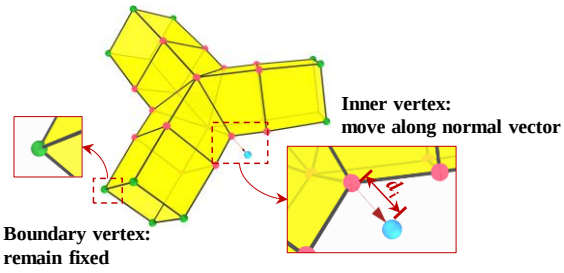

Figure 3 The adjustment of the control mesh

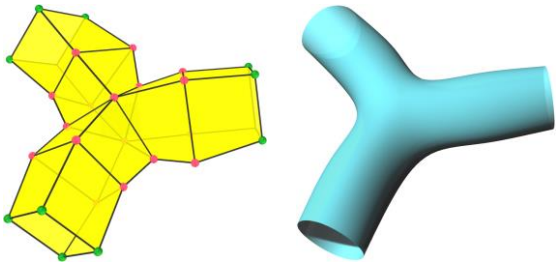

(a) Control mesh (b) Subdivision surface

Figure 4 Deformed joint shape

The displacement of vertex i along the normal direction is defined as the shape parameters and denoted as d_i. Since the joint's shape is determined by the shape parameters (d_i) of all vertices, they are selected as the design variables of the shape optimization problem.

2.3. Structural analysis

The structural analysis module is developed through secondary development in Abaqus software, and its process is demonstrated in Figure 5 Initially, this module imports the geometric models and configures the material properties. In this research, a linear elastic material model is utilized, with the elastic modulus for cast steel set at 2.06×10^5 MPa. Subsequently, the finite element mesh is generated with the mesh size determined by sensitivity analysis. Given the study's emphasis on CST joints with uniform wall thickness, shell elements are selected. Following this, the boundary conditions and loads are applied, according to the realistic conditions of the joint. The process concludes with performing the finite element analysis, from which the results are extracted and prepared for the optimization algorithm module.

2.4. Optimization algorithm

In this research, the design variables are the shape parameters d_i, while the objective is the maximum Mises stress or strain energy of the joint. Due to the complexity of determining their mathematical relationship and the challenge of obtaining gradient information, the gradient-free genetic algorithm is adopted to solve the optimization problem.

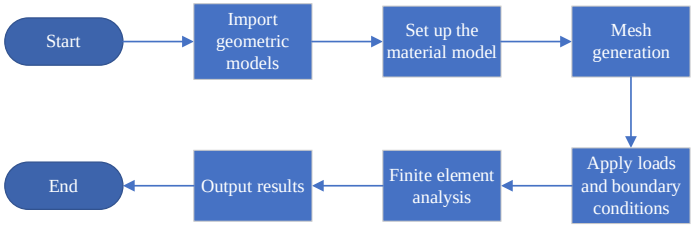

Figure 5 The procedure of the structural analysis module

The genetic algorithm begins with population initialization, where a set of individuals are randomly generated, with their fitness evaluated. Following this, the genetic operators are applied to the population. The selection operator determines which individuals continue to participate in the subsequent reproduction process, the crossover operator combines the genes of the parent individuals, and the mutation operator is responsible for maintaining the diversity of the population. Specifically, this study utilizes tournament selection for choosing individuals, uniform crossover for combining genes, and uniform mutation for introducing variability. After these genetic manipulations, an offspring population emerges and is subjected to repeated iterations until meeting the stopping criterion.

3. Numeric examples

3.1. Stress optimization of a three-member joint

3.1.1. Joint configuration

The dimensions of the joint are depicted in Figure 6. This joint connects three members, all situated within the same plane. The upper members have a cross-section of D350 × 20 mm, whereas the cross-section of the lower member is D420 × 20 mm. Each of the upper members is subject to an axial force of 1000 kN at their ends, while the lower member is fully fixed, as demonstrated in Figure 7.

Utilizing the geometric modeling approach outlined in Section 2.2, the initial shape of the joint is established, from which its control mesh is derived, as illustrated in Figure 8 The control mesh comprises a total of 29 vertices, with 12 positioned along the mesh boundary. These boundary vertices remain fixed during the optimization process. Given the joint's symmetry, the configuration of the joint is fully defined by the position of 7 internal vertices (marked as blue vertices in Figure 8(a)). Therefore, the shape parameters d_i of these 7 vertices are selected as the design variables for the optimization problem.

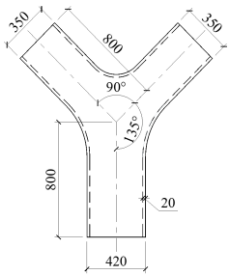

Figure 6 Joint dimensions

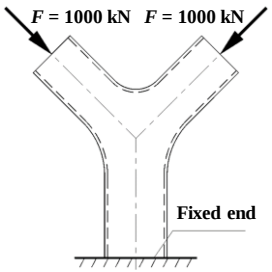

Figure 7 Loads of the joint

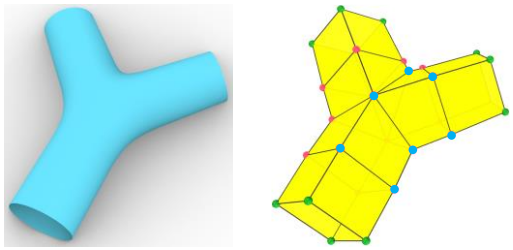

(a) Subdivision surface (b) Control mesh

Figure 8 Initial shape of the joint

3.1.2. Optimization formulation and solution

In this problem, the shape parameters (d_i) are used as the design variables, and the maximum Mises stress of the joint is used as the objective function. Meanwhile, a penalty term for the joint volume is added to the objective function to avoid excessive increases in the joint volume. Thus, the optimization formulation of the problem is obtained as

$$\begin{aligned} \min \quad & f\left(d_i\right)=\frac{\sigma_{\max}}{\sigma_0}+\alpha\times\max\left(\frac{V}{V_0}-1.2\ ,\ 0\right) \\ \text{s.t.} \quad & -150\le d_i\le 150 \\ & \left(i=1,2,\cdots,7\right) \end{aligned} \tag{1}$$

In equation (1), d_i is the shape parameter of vertex i. $\sigma_{\max}$ and σ_0 are the maximum Mises stress of the current joint and the initial joint, respectively. α is the penalty coefficient which is taken as 5, while V and V_0 are the volume of the current and initial joints, respectively.

The genetic algorithm is adopted to solve the optimization problem, with its parameters exhibited in Table 1.

3.1.3. Optimization results

Three shape optimization trials are conducted for the joint, with the changes in minimum fitness across each trial presented in Figure 9 The minimum fitness experiences a sharp decline within the initial 15 generations, followed by a more gradual decrease post the 15th generation. Upon completing 30 generations of iterations, the fitness levels of the optimal individuals from the three trials are recorded as 0.377, 0.399, and 0.401, respectively. For further analysis, the optimal individual from the first trial is selected as the optimized joint configuration.

Table 1 Parameters of the genetic algorithm

Parameter	Value	Detail
Population size	30	
Maximum iteration	30	
Selection operator	Tournament	Tournament size: 3
Crossover operator	Uniform crossover	Crossover probability: 0.5
Mutation operator	Uniform mutation	Mutation probability: 0.3

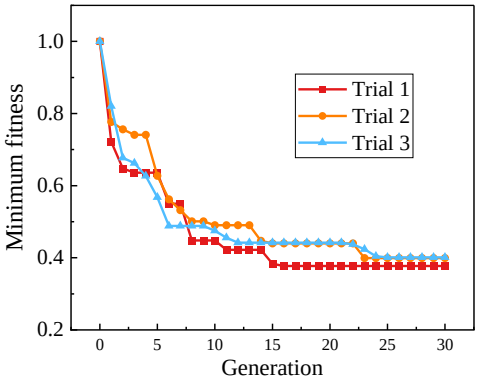

Figure 9 Minimum fitness in the optimization process

The configurations of the initial and optimized joints are depicted in Figure 10. Figure 10 reveals significant changes in the optimized joint's shape, with the central section contracting inward. Furthermore, the initial joint's volume stands at 5.33×10^7 mm^3, whereas the optimized joint's volume reduces to 4.94×10^7 mm^3, aligning with the constraints on joint volume.

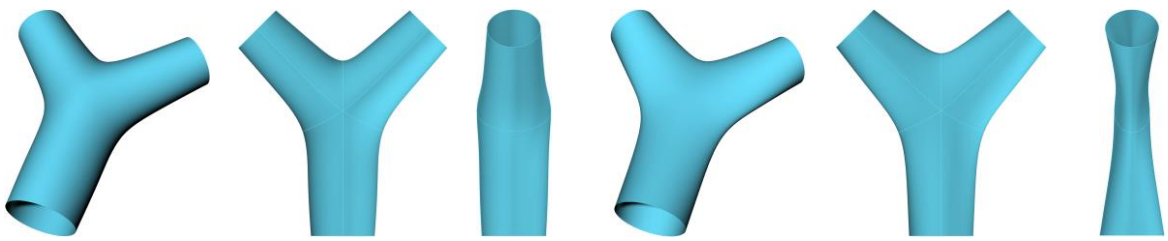

(a) The initial joint (b) The optimized joint

Figure 10 Joint shape

The Mises stress contours for the initial and optimized joints are illustrated in Figure 11. The initial joint exhibits a maximum Mises stress of 195.2 MPa, in contrast to the optimized joint's maximum stress of 73.61 MPa—merely 37.7% of the initial value. This substantial reduction in the maximum Mises stress of the optimized joint underscores the efficacy of the proposed shape optimization method.

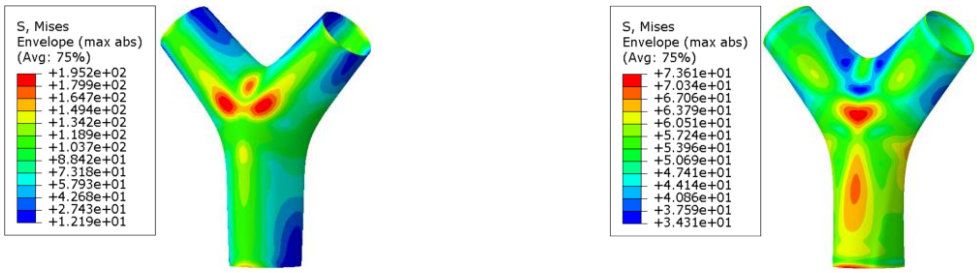

(a) The initial joint (b) The optimized joint

Figure 11Mises stress contour

3.2. Strain energy optimization of a four-member joint

3.2.1. Joint configuration

The configuration of the joint in this example is depicted in Figure 12. It connects four members: the lower member has a cross-section of D410×15 mm, while the upper members each have a cross-section of D270×15 mm. Each of the three upper members is subjected to an axial force of 240 kN and a bending moment of 50 kN·m, as illustrated in Figure 13.

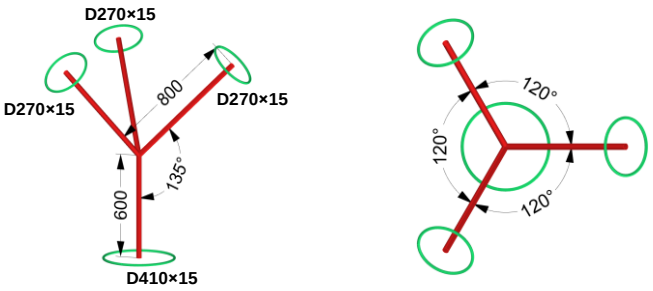

(a) Perspective view (b) Top view

Figure 12 Dimensions of the joint

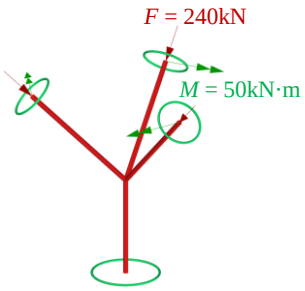

Figure 13 Loads of the joint

Based on the geometric modeling approach described in section 2.2, the initial joint shape is constructed and its control mesh is extracted as shown in Figure 14. This control mesh comprises 26 vertices, including 16 end vertices that remain fixed throughout the shape optimization process. Given the joint's symmetry, its shape is fully defined by the placement of 4 vertices (marked as blue vertices in Figure 14). Therefore, the shape parameters of these 4 vertices are designated as the design variables for the shape optimization task.

(a) Subdivision surface (b) Control mesh

Figure 14 Initial shape of the joint

3.2.2. Optimization formulation

In the shape optimization task, the shape parameters d_i of the four vertices are taken as the design variables, and the strain energy of the joint is selected as the objective. A penalty term for joint volume is also added to the objective function. Thus, the optimization formulation is obtained as equation (2).

$$\begin{aligned} \min \quad & f\left(d_i\right)=\frac{E}{E_0}+\alpha\times\max\left(\frac{V}{V_0}-1.2\ ,\ 0\right) \\ \text{s.t.} \quad & -150\le d_i\le 150 \\ & \left(i=1,2,3,4\right) \end{aligned} \tag{2}$$

In equation (2), E and E_0 are the strain energy of the current and initial joint, respectively. The meanings and values of the remaining parameters are the same as those in equation (1). The genetic algorithm is utilized to solve the optimization problem, with the parameters detailed in Table 1.

3.2.3. Optimization results

Three shape optimization trials are carried out, with the population's minimum fitness depicted in Figure 15. In each trial, the minimum fitness sharply declines within the initial 10 generations and remains nearly unchanged in the subsequent iterations. By the 30th generation, the minimum fitness values recorded for the three trials are 0.457, 0.435, and 0.439, respectively. The optimal individual derived from the second trial is selected as the optimized joint for further analysis.

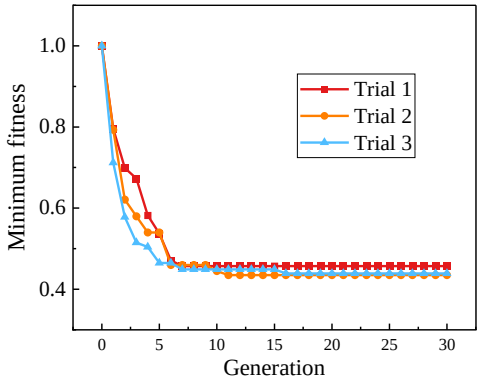

Figure 15 Minimum fitness variation

Figure 16 displays the shapes of the initial and optimized joints. There is a marked difference in the shape of the optimized joint compared to the initial one. The optimized joint exhibits significant inward contraction at the junctures where the branches meet, as indicated by the red arrows. Meanwhile, the volume of the optimized joint remains close to that of the initial design, marginally increasing to approximately 103.5% of the initial value, which aligns with the specific volume limits.

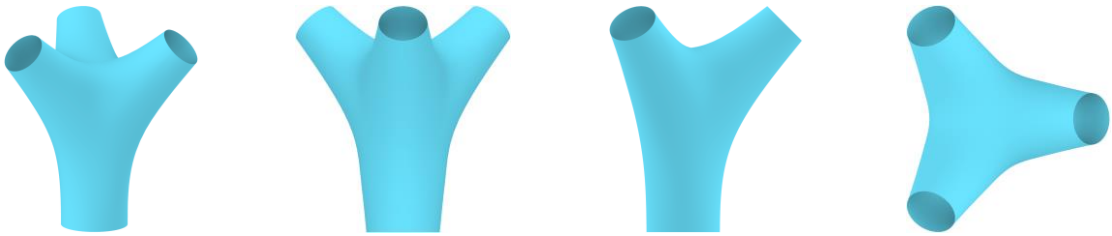

(a) The initial joint

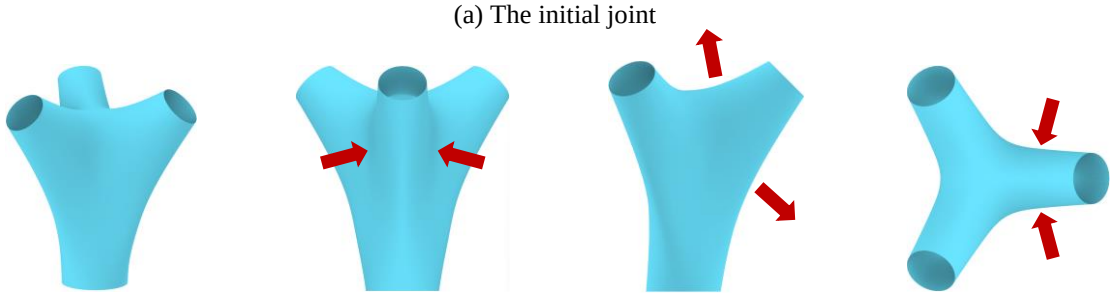

(b) The optimized joint

Figure 16 The shape of the initial and optimized joints

Figure 17 presents the strain energy density contours for the initial and optimized joints. The optimized joint demonstrates a notably more even distribution than the initial joint. Meanwhile, the total strain energy of the initial and optimized joints is 243.4 N·m and 105.8 N·m, indicating a 56.5% reduction in the optimized joint. Concurrently, Figure 18 illustrates the Mises stress contours for both joints, highlighting a marked decrease in peak stress levels. The initial joint's maximum Mises stress is 204.2 MPa, whereas the optimized joint displays a reduction to 87.3 MPa—42.8% of the initial value. These marked improvements in strain energy density and Mises stress underscore the efficacy of the shape optimization method applied.

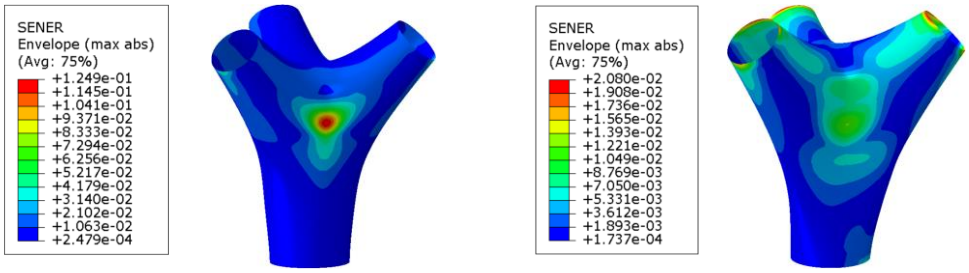

(a) The initial joint (b) The optimized joint

Figure 17 The strain energy density contour

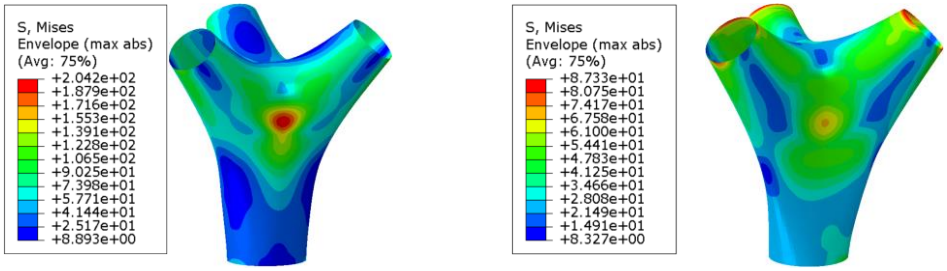

(b) The initial joint (b) The optimized joint

Figure 18 The Mises stress contour

4. Conclusion

In this study, we introduced an innovative shape optimization framework for CST joints, utilizing the subdivision surface technique and genetic algorithm. The shape optimization framework comprises three critical modules- geometric modeling, structural analysis, and optimization algorithm- to streamline the design process of CST joints. The geometric module provides smooth CST joint designs with a few shape parameters to control the joint shape, the structural analysis module conducts finite element analysis for the CST joints automatically, and the optimization algorithm module performs genetic algorithms and adjusts the shape parameters.

The proposed shape optimization framework is implemented on two CST joints, taking the maximum Mises stress and strain energy as the optimization objectives, respectively. This approach results in substantial shape changes of the joints, highlighting the framework's flexible shape control capabilities. Meanwhile, the framework achieved a 62.3% reduction in Mises stress and a 56.5% reduction in strain energy across the two case studies, illustrating a significant enhancement in the joints' mechanical performance.

The proposed framework offers notable merits compared to the traditional trial-and-error design approach and the topology optimization methods. Initially, the proposed framework can effectively reduce the stress level and strain energy, significantly improving the design quality of the CST joints. Subsequently, the proposed framework is highly automated and considerably reduces the labor intensity involved in the design process. Finally, it ensures that joint designs have a continuous, smooth surface, thus resolving manufacturability issues brought about by the topology optimization methods.

While this study mainly focuses on the shape optimization of CST joints with uniform wall thickness, further research can explore the shape optimization of CST joints with varied wall thickness to expand the application scope of the proposed framework.

References

[1] W. Pietraszkiewicz and V. Konopińska, "Junctions in shell structures: A review," *Thin-Walled Struct.*, vol. 95, pp. 310–334, Oct. 2015, doi: 10.1016/j.tws.2015.07.010.

[2] S. Bao, W. Wang, J. Zhou, S. Qi, and X. Li, "Experimental study of hot spot stress for three-planar tubular Y-joint: I. Basic loads," *Thin-Walled Struct.*, vol. 177, p. 109418, Aug. 2022, doi: 10.1016/j.tws.2022.109418.

[3] T. Urbański and M. Taczała, "Prediction of the welding distortions of butt welded joints using total moments method based on equivalent loads," *J. Manuf. Process.*, vol. 75, pp. 1039–1057, Mar. 2022, doi: 10.1016/j.jmapro.2022.01.053.

[4] Z. Wei, X. Pei, and H. Jin, "Evaluation of welded cast steel joint fatigue data using structural stress methods," *J. Constr. Steel Res.*, vol. 186, p. 106895, Nov. 2021, doi: 10.1016/j.jcsr.2021.106895.

[5] L. Wang, W. Du, P. He, and M. Yang, "Topology Optimization and 3D Printing of Three-Branch Joints in Treelike Structures," *J. Struct. Eng. U. S.*, vol. 146, no. 1, 2020, doi: 10.1061/(ASCE)ST.1943-541X.0002454.

[6] S. Huang, X. Deng, and L. K. Lam, "Integrated design framework of 3D printed planar stainless tubular joint: Modelling, optimization, manufacturing, and experiment," *Thin-Walled Struct.*, vol. 169, p. 108463, Dec. 2021, doi: 10.1016/j.tws.2021.108463.

[7] S. Huang, X. Deng, and Y. Wang, "Experimental investigations of optimized 3D Printing Planar X-joints manufactured by stainless steel and high-strength steel," *Eng. Struct.*, vol. 285, p. 116054, Jun. 2023, doi: 10.1016/j.engstruct.2023.116054.

[8] W. Zuo, M.-T. Chen, Y. Chen, O. Zhao, B. Cheng, and J. Zhao, "Additive manufacturing oriented parametric topology optimization design and numerical analysis of steel joints in gridshell structures," *Thin-Walled Struct.*, vol. 188, p. 110817, Jul. 2023, doi: 10.1016/j.tws.2023.110817.

[9] M.-T. Chen, W. Zuo, Y. Chen, O. Zhao, B. Cheng, and J. Zhao, "Parametric topology optimization design and analysis of additively manufactured joints in spatial grid structures," *Eng. Struct.*, vol. 300, p. 117123, Feb. 2024, doi: 10.1016/j.engstruct.2023.117123.

[10] J. Liu and Y. Ma, "A survey of manufacturing oriented topology optimization methods," *Adv. Eng. Softw.*, vol. 100, pp. 161–175, Oct. 2016, doi: 10.1016/j.advengsoft.2016.07.017.

[11] S. C. Subedi, C. S. Verma, and K. Suresh, "A Review of Methods for the Geometric Post-Processing of Topology Optimized Models," *J. Comput. Inf. Sci. Eng.*, vol. 20, no. 6, Art. no. 6, Dec. 2020, doi: 10.1115/1.4047429.

[12] L. Xia, L. Zhang, Q. Xia, and T. Shi, "Stress-based topology optimization using bi-directional evolutionary structural optimization method," *Comput. Methods Appl. Mech. Eng.*, vol. 333, pp. 356–370, May 2018, doi: 10.1016/j.cma.2018.01.035.

[13] Y. Ding, "Shape optimization of structures: a literature survey," *Comput. Struct.*, vol. 24, no. 6, Art. no. 6, 1986, doi: 10.1016/0045-7949(86)90307-X.

[14] A. Francavilla, C. V. Ramakrishnan, and O. C. Zienkiewicz, "Optimization of shape to minimize stress concentration," *J. Strain Anal.*, vol. 10, no. 2, Art. no. 2, Apr. 1975, doi: 10.1243/03093247V102063.

[15] R. T. Haftka and R. V. Grandhi, "Structural shape optimization—a survey," *Comput. Methods Appl. Mech. Eng.*, vol. 57, no. 1, Art. no. 1, 1986.

[16] K.-U. Bletzinger, S. Kimmich, and E. Ramm, "Efficient modeling in shape optimal design," *Comput. Syst. Eng.*, vol. 2, no. 5, pp. 483–495, Jan. 1991, doi: 10.1016/0956-0521(91)90051-6.

[17] V. Braibant and C. Fleury, "Shape optimal design using B-splines," *Comput. Methods Appl. Mech. Eng.*, vol. 44, no. 3, Art. no. 3, Aug. 1984, doi: 10.1016/0045-7825(84)90132-4.

[18] U. Schramm and W. D. Pilkey, "The coupling of geometric descriptions and finite elements using NURBs — A study in shape optimization," *Finite Elem. Anal. Des.*, vol. 15, no. 1, Art. no. 1, Dec. 1993, doi: 10.1016/0168-874X(93)90067-Z.

[19] G. M. Chaikin, "An algorithm for high-speed curve generation," *Comput. Graph. Image Process.*, vol. 3, no. 4, pp. 346–349, Dec. 1974, doi: 10.1016/0146-664X(74)90028-8.

[20] C. LOOP, "Smooth Subdivision Surfaces Based on Triangles," *Masters Thesis Univ. Utah Dep. Math.*, 1987.

[21] D. Doo and M. Sabin, "Behaviour of recursive division surfaces near extraordinary points," in *Seminal graphics*, New York, NY, USA: ACM, 1998, pp. 177–181. doi: 10.1145/280811.280991.

[22] E. Catmull and J. Clark, "Recursively generated B-spline surfaces on arbitrary topological meshes," in *Seminal graphics*, New York, NY, USA: ACM, 1998, pp. 183–188. doi: 10.1145/280811.280992.